

PAPER • OPEN ACCESS

Detection of low-energy charged particles by channel electron multipliers

To cite this article: D.M. Newson et al 2022 JINST 17 P11026

View the <u>article online</u> for updates and enhancements.





RECEIVED: August 16, 2022 Accepted: October 26, 2022 Published: November 18, 2022

Detection of low-energy charged particles by channel electron multipliers

D.M. Newson, a M. Shipman, a S.J. Brawley, a R. Kadokura, a T.J. Babij, b D. Cooke, a D.E. Leslie a and G. Laricchia a,*

^a UCL Department of Physics and Astronomy, University College London, Gower Street, London WC1E 6BT, U.K.

E-mail: g.laricchia@ucl.ac.uk

ABSTRACT: Experimental determinations of the detection efficiency for positrons impacting a channel electron multiplier with incident energies between 0–1400 eV are presented. A log-normal dependence with energy is established and used to compute the positron-to-positronium detection efficiency ratio as a function of positronium energy, as required for determining quantities involving the ratio of positron and positronium rates. A log-normal energy-dependence is also observed in results of previous work with electrons, protons and ions.

Keywords: Analysis and statistical methods; Detector modelling and simulations I (interaction of radiation with matter, interaction of photons with matter, interaction of hadrons with matter, etc); Detector modelling and simulations II (electric fields, charge transport, multiplication and induction, pulse formation, electron emission, etc); Electron multipliers (vacuum)

^b Research School of Physics and Engineering, Australian National University, Canberra, ACT 2600, Australia

^{*}Corresponding author.

1	Introduction]
2	Detectors & method	2
3	Results & analysis	
	3.1 Experimental measurements	
	3.2. Statistical description	

1 Introduction

Conclusions & outlook

Contents

Channel electron (e^-) multipliers are important tools in the detection of particles in a variety of environments on Earth [1] and in space [2]. The detection efficiencies of such devices, from the impact of ions, atoms and molecules, have been studied extensively and predictive relationships, with energy, velocity or mass of the incident projectiles, proposed ([3–6] and references therein). In the case of positrons (e^+), investigations of the single channel electron multiplier (CEM) detection efficiency (ε_+^d) available in the literature are scarce, covering impact energies 50–1200 eV [7] and 3–30 keV [8].

For positronium (Ps), the short-lived $e^- - e^+$ bound-state, direct determinations of the detection efficiency (ε_{Ps}^d) are limited to channel-electron-multiplier-arrays (CEMA) and impact energies between 13–33 eV [9, 10] where it was found to be consistent, within errors, with that for equivelocity e^+ , i.e. ε_{Ps}^d was approximately equal to ε_+^d evaluated at $E_{Ps}/2$ where E_{Ps} is the Ps kinetic energy.

The ratio of e^+ and Ps detection efficiencies, $R_d = \varepsilon_+^d/\varepsilon_{\rm Ps}^d$, is required, for example, to determine absolute cross-sections for differential Ps-formation [11, 12] and Ps fragmentation in collision with atoms [10, 13]. Whilst the absolute magnitudes of ε_+^d and $\varepsilon_{\rm Ps}^d$ depend on the detector, its age and the electronic settings of the system, the ratio R_d has been found in general not to change significantly [14].

Following a brief description of the apparatus, new experimental determinations of ε_+^d are presented and compared with previous work [15–17] for incident energies between 0–1400 eV. Systematic effects are understood with the aid of simulations, allowing the data to be reconciled into a single curve that shows a clear log-normal energy dependence [18]. R_d is extracted by first fitting a log-normal function to current and previous ε_+^d in combination and then implementing the equivelocity relationship to determine $\varepsilon_{P_8}^d$ [9, 10, 19]. The energy dependence of the detection efficiency of e^+ [7], e^- [20], protons [21] and positive ions [6, 21] from previous investigations are also examined and found to be well described by log-normal functions.

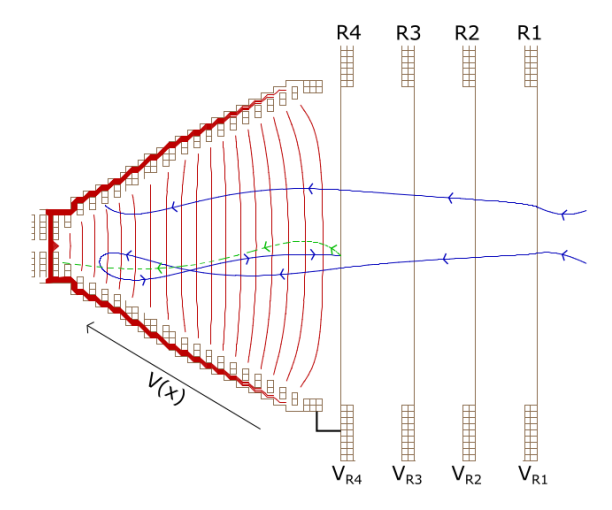


Figure 1. Schematic diagram of the detection system, comprising a CEM and four 90% transmission tungsten grids R1, R2, R3 and R4, the latter connected to the cone to minimise $\vec{E} \times \vec{B}$ effects. Equipotential contours (solid) are shown for the case $V_{R4} = -70 \text{ V}$, in steps of 5 V inside the cone. Trajectories, simulated in SIMION, are illustrated for two e^+ (solid with arrowhead) along with that for an SE (dashed with arrowhead) liberated from R4 due to e^+ reflected by V(x) (see text).

2 Detectors & method

The e^+ beam lines at UCL have been described in detail elsewhere, e.g. [16, 22]. Briefly, β^+ particles from the decay of 22 Na are moderated by a thin layer of rare gas (Kr or Ne) frozen directly onto the source capsule or by an annealed W grid, producing slow e^+ that are accelerated by a variable positive potential applied to the moderator and confined radially by an axial magnetic field. An $\vec{E} \times \vec{B}$ filter separates the e^+ beam from fast particles and removes the line of sight between source and detectors. The beam line described in [22] is also used to generate a Ps beam.

 e^+ , e^- , ions, Ps and other neutral particles can be detected through the multiplication of secondary electrons (SE) released upon impact with an emissive surface. In the case of a CEM, the surface of initial impact takes the form of a cone with base diameter large compared to that of the channel. For the detection of charged particles, typically a potential of opposite polarity to the projectile charge accelerates them into the emissive layer coating the cone and channel, releasing SE. A positive bias applied to the back of the CEM (V_{back}) then causes SE to impact the emissive layer, releasing yet more SE. The channel geometry ensures many impacts occur, causing an avalanche of SE that are collected at the end of the channel by a positively-biased electrode, generating a current pulse that can be amplified and detected.

The CEM employed in this study is a KBL25RS/90 CEM from Dr. Sjuts [23] with 25 mm diameter cone, placed behind four W grids through which the beam travels, as shown in figure 1. For detection of e^+ , R1 is grounded and the grids R2 and R3 are typically held at $V_{R2} = V_{R4} - 150 \text{ V}$ and $V_{R3} = V_{R4} - 50 \text{ V}$ respectively, to reflect SE emitted from the CEM surface towards the grids, thereby increasing the detection efficiency. R4 is connected to the edge of the cone and therefore all potentials are set by V_{R4} . V(x), where x is the point of impact on the surface of the cone, is the linearly increasing potential from the base to the apex of the cone [24].

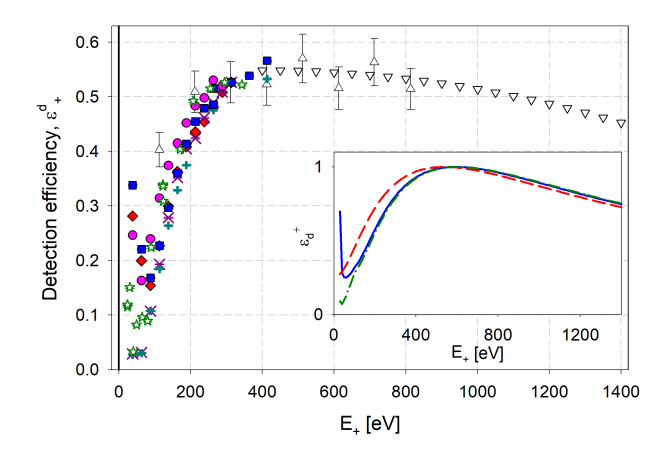


Figure 2. Present ε_+^d measurements obtained using a CEM with 25 mm diameter cone as a function of E_+ with grids R2 and R3 biased (filled symbols) and grounded (cross, plus and star symbols) alongside previous measurements using a CEM with 10 mm diameter cone (hollow up triangle) [15, 16] and (hollow down triangle) [17]. Also shown in the inset are simulation results, normalised to peak of unity, for e^+ interacting with the grids and 25 mm CEM cone with voltages applied to R2 and R3 with (solid line) and without (dashed line) accounting for V(x) (see text), and with R2 and R3 grounded and V(x) (dot-dashed line).

Positrons are detected by impact with the CEM in coincidence with an annihilation γ -ray registered by a CsI scintillator located behind the CEM, e.g. [22]. ε_+^d can be determined by performing coincidence measurements between the CEM and the CsI, and is given by $\varepsilon_+^d = N_c/N_\gamma$ where N_c is the coincidence rate and N_γ the count rate recorded simultaneously on the CsI detector, with both quantities net of backgrounds, e.g. [25].

The e^+ impact energy (E_+) can be controlled by either maintaining a fixed negative potential applied to the cone (V_{R4}) and varying the incident e^+ beam energy (E_{inc}) , or by keeping E_{inc} constant and varying V_{R4} . In the present study, to keep the e^+ beam intensity approximately constant across the energy range investigated, the latter method was employed. In both cases the e^+ energy at R4 is given by $E_+ = E_{inc} - eV_{R4}$.

3 Results & analysis

3.1 Experimental measurements

New measurements of ε_+^d as a function of E_+ are shown in figure 2 alongside previous work of Cooke et al. [15, 16] and Laricchia et al. [17], both employing a CEM with 10 mm diameter cone. For shape comparison, the data of Laricchia et al. were normalised to the mean of Cooke et al. around the peak and the current data normalised to Cooke et al. at $\simeq 300 \, \text{eV}$. The different filled symbols correspond to measurements under slightly different experimental conditions (axial magnetic field, E_{inc} , etc.). Reasonable agreement is found amongst those with voltages applied to R2 and R3 and, separately, those with R2 and R3 grounded.

For E_+ between 0.1–1.4 keV, ε_+^d increases with energy up to a peak at $\simeq 450$ eV before decreasing slowly towards higher energies. Additionally, ε_+^d is found to increase below $\simeq 0.1$ keV. This feature has been reproduced in a Monte Carlo simulation of e^+ impacting the W grids and CEM [19], the

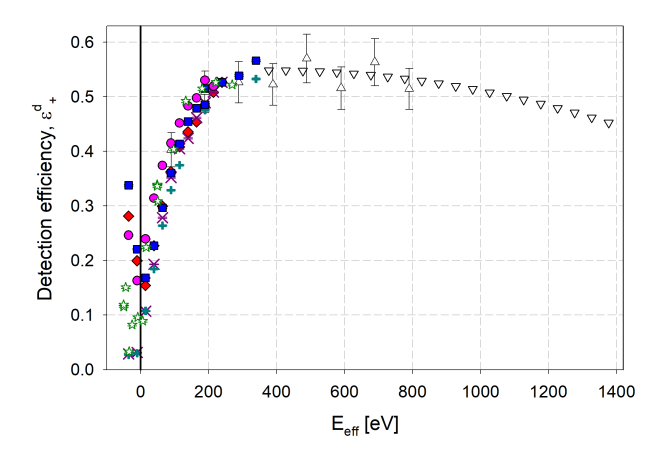


Figure 3. Current and previous [15–17] ε_+^d determinations (symbols as in figure 2) shifted by 74 eV and 23 eV, as determined by simulation for 25 mm and 10 mm diameter CEM cones, respectively (see text).

results of which for a 25 mm diameter cone with R2 and R3 biased and with both grounded are shown in the inset of figure 2. Besides those produced upon impact with the cone, SE are also generated from e^+ impacting the grids, that are then accelerated into the cone at increasing energies as $|V_{R4}|$ is reduced. The detection efficiency is related to the SE yield from the cone, which for a range of materials has been found to follow a log-normal distribution [26], and rises sharply as E_+ increases. SE generated at R4 are always accelerated towards the CEM because the cone is positive with respect to R4, thus contributing to the non-zero offset in ε_+^d . When R2 and R3 are grounded, the rise of ε_+^d towards lower E_+ is reduced because SE from these grids are reflected by V_{R4} .

A displacement in energy is noted between measurements of the current work employing a CEM with a 25 mm diameter cone and the previous work performed with a 10 mm diameter cone. Results of simulation (inset of figure 2) for a 25 mm cone, have confirmed the shift to be due to V(x) which gives an *effective* impact energy $E_{\text{eff}} = E_+ - eV(x)$. The observed shift is related to V(x) averaged over the illuminated part of the cone $\langle V(x) \rangle$. In all measurements, the gain, set by the voltage across the CEM $(V_{\text{back}} - V_{\text{R4}})$, was kept constant as V_{R4} was varied, therefore $\langle V(x) \rangle$ was fixed for a given cone geometry. Shifts of $\simeq 74 \, \text{eV}$ and $\simeq 23 \, \text{eV}$ were determined by simulation for a centred 4 mm diameter e^+ beam impacting the 25 mm and 10 mm diameter cones, respectively [19].

Figure 3 shows ε_+^d shifted by the amounts determined from simulation. The rise of ε_+^d at negative $E_{\rm eff}$, can be understood as being predominantly due to e^+ that are reflected by V(x), subsequently colliding with the grids and generating SE that impact the cone, as illustrated in figure 1.

3.2 Statistical description

General relationships between impact energy and detection efficiency have been investigated previously for ions, through scaling of the energy by velocity [5] and mass [3, 6]. Seah et al. [4], in their model approach, scaled by the energy of maximum efficiency. Here, for ε_+^d , we are guided by recent findings regarding the log-normal distribution as a description of inelastic collisions as a function of the excess energy $E' = E - E_{th}$, where E_{th} is the threshold energy for the process under consideration [18]. In the present case, $E = E_{eff}$ and the threshold for detection is the work

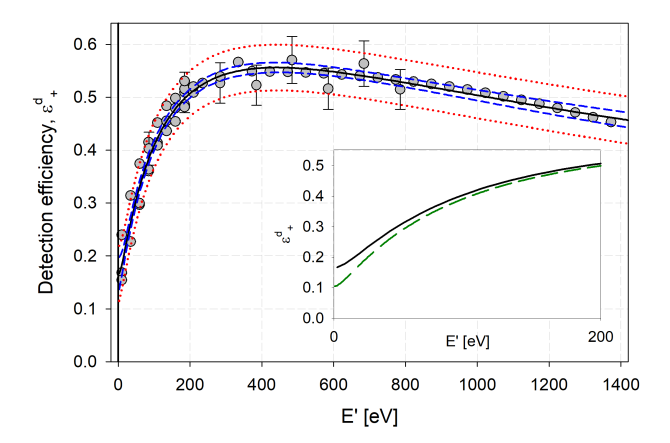


Figure 4. Log-normal fit (solid line, $R^2 = 0.97$) to ε_+^d for biased grids of figure 3 with the work function of the detector surface deducted (bullets). Also shown are 95% confidence (dotted line) and prediction (dashed line) bands. In the inset, this result is compared with the log-normal fit (dashed line) to ε_+^d obtained with grounded grids in combination with the high energy points of [17]. The fit parameters in both cases are listed in table 1.

function (ϕ) of the CEM surface, estimated as 4.5 eV based on the Ni and Pb content of the cone material [27]. Figure 4 shows a 4-parameter log-normal fit, of form

$$f(E') = y_0 + \frac{a}{E'} \exp\left[-\frac{1}{2} \left(\frac{\ln\left(\frac{E'}{x_0}\right)}{b}\right)^2\right],\tag{3.1}$$

to the positive E' data obtained with biased grids, together with 95% confidence and prediction bands. In the inset, the fit is compared with that obtained from measurements with R2 and R3 grounded in combination with the high energy points of [17]. The parameters extracted from both fits are listed in table 1. The non-zero value of y_0 reflects the constant contribution to the detection efficiency from SE released from the grids in both cases. It is smaller when R2 and R3 are grounded as only R4 contributes SE in this case.

The detection efficiency ratio $R_d = \varepsilon_+^d/\varepsilon_{\rm Ps}^d$ as a function of $E_{\rm Ps}$ is shown in figure 5. It was determined from f(E') and the extracted fit parameters by setting ε_+^d as the mean positron detection efficiency between 250–600 eV, corresponding to the range of beam energies typically used in fragmentation and differential Ps-formation cross-section measurements [10–12], and by extracting $\varepsilon_{\rm Ps}^d$ using the equivelocity relationship [9, 10, 19].

In figure 6(a), detection efficiencies determined in previous work for e^+ [7], e^- [20] and protons [21, 23] are shown. Because of insufficient information, the data are plotted versus the nominal energy E rather than $E' = (E - eV(x) - \phi)$. Although there are considerable discrepancies among measurements for e^- reported in the literature, those of Bordoni [20] broadly agree with the results of Philips [21] and Dr. Sjuts [23] (not included in the figure for clarity). Figure 6(b) displays the detection efficiency for Ne⁺, Ar⁺, Kr⁺, Xe⁺, and the combinations O₂⁺ and O⁺, and N₂⁺ and N⁺, determined by Krems et al. [6]. Due to the lack of biased grids, no offset was expected in the results of Sueoka [7], Krems et al. [6], Philips [21] and Bordoni [20], therefore a 3-parameter

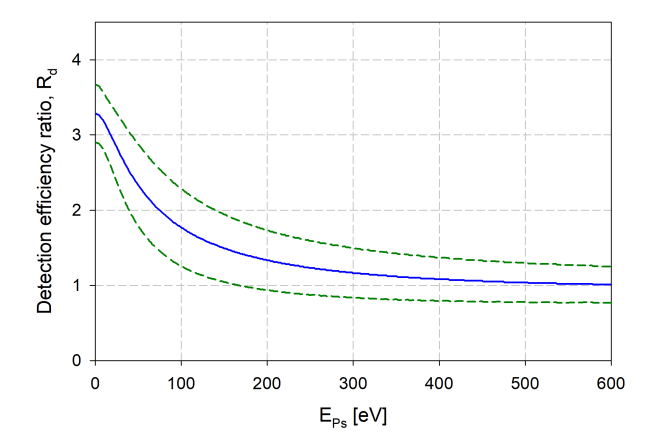


Figure 5. R_d as a function of E_{Ps} (solid). The standard error, propagated from the uncertainty of the fit parameters, is also displayed (dashed).

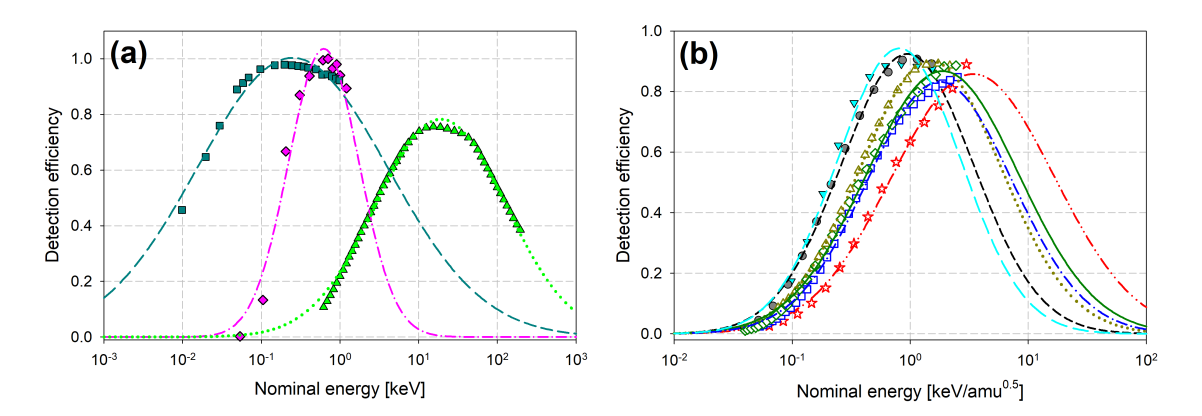


Figure 6. (a) Detection efficiencies as a function of nominal energy (see text): e^+ , Sueoka [7] (diamond); e^- , Bordoni [20] (square); protons, Philips [21] (up triangle). Also shown are log-normal fits (lines) to the corresponding data: e^+ (dot-dashed); e^- (dashed); protons (dotted). (b): positive ion detection efficiencies of Krems et al. [6]: O_2^+ and O_2^+ (circle); O_2^+ and O_2^+ (down triangle); O_2^+ (up triangle); O_2^+ (square); O_2^+ (diamond); O_2^+ (star), alongside log-normal fits to the corresponding data: O_2^+ and O_2^+ (long dashed); O_2^+ and O_2^+ (short dashed); O_2^+ (dot-dashed); O_2^+ (solid); O_2^+ (double-dot-dashed). The parameters extracted from the fits are listed in table 1.

log-normal function was used and found to describe the data well, except at low energies where deviations may be noted arising from the use of E rather than E'. The extracted fit parameters are included in table 1.

4 Conclusions & outlook

Experimental determinations of the CEM e^+ detection efficiency have been presented for energies between 0–1400 eV. A log-normal energy dependence of the detection efficiencies of e^+ , e^- , protons and ions has been established. The ratio of the e^+ and Ps detection efficiencies has been extracted using a log-normal fit to current and previous CEM e^+ detection efficiency measurements in combination with the equivelocity relationship [9, 10, 19] and with typical voltages applied to the CEM

Table 1. Parameters extracted from log-normal fits to ε_+^d of the current work, shown in figure 4, and those from previous studies, shown in figures 6(a) and 6(b). The 3-parameter log-normal (equation (3.1) with $y_0 = 0$) was fit to data in all cases except those from this study where the 4-parameter function was applied due to the constant contribution to ε_+^d from R4.

Projectile	а	b	x_0	У0
e ⁺ (biased grids)	$(5.50 \pm 0.82) \times 10^2$	1.53 ± 0.07	$(4.51 \pm 1.05) \times 10^3$	0.17 ± 0.02
e^+ (grounded grids)	$(8.00 \pm 1.61) \times 10^2$	1.65 ± 0.09	$(6.91 \pm 2.28) \times 10^3$	0.10 ± 0.02
e ⁺ [7]	1.10 ± 0.12	1.03 ± 0.08	1.81 ± 0.36	
e^{-} [20]	12.1 ± 4.2	2.79 ± 0.11	$(5.84 \pm 3.87) \times 10^2$	-
Protons [21]	91.4 ± 2.8	1.90 ± 0.02	$(7.11 \pm 0.45) \times 10^2$	-
O ₂ ⁺ and O ⁺ [6]	2.00 ± 0.17	1.29 ± 0.04	4.95 ± 0.64	-
N_2^+ and N^+ [6]	1.58 ± 0.18	1.21 ± 0.06	3.49 ± 0.65	-
Ne ⁺ [6]	3.48 ± 0.10	1.38 ± 0.01	10.0 ± 0.4	-
Ar ⁺ [6]	4.03 ± 0.29	1.41 ± 0.03	13.2 ± 1.4	-
Kr ⁺ [6]	4.94 ± 0.49	1.49 ± 0.03	17.3 ± 2.4	-
Xe ⁺ [6]	10.2 ± 2.4	1.58 ± 0.07	41.7 ± 13.6	-

cone and grids. The goodness of the log-normal fits ($R^2 \ge 0.95$) to data for a variety of projectiles with different charge and mass provide additional evidence in support of the conclusions drawn by Laricchia et al. [18], that such a statistical function may also describe the energy dependence of inelastic collisions at the quantum level.

Acknowledgments

The authors wish to thank John Dumper, Rafid Jawad and Derek Thomas for their valuable assistance. The Engineering and Physical Sciences Research Council is gratefully acknowledged for supporting this work under grant numbers EP/P009395/1, EP/R513143/1 and for providing DMN with a research studentship. TJB is grateful for The Robert and Helen Crompton Award. For the purpose of open access, the corresponding author has applied a Creative Commons Attribution (CC BY) licence to any Author Accepted Manuscript version arising from this submission. The data that support the findings of this study are openly available at UCL Discovery.¹

References

- [1] T. Gys, Micro-channel plates and vacuum detectors, Nucl. Instrum. Meth. A 787 (2015) 254.
- [2] H.O. Funsten et al., Comparative response of microchannel plate and channel electron multiplier detectors to penetrating radiation in space, IEEE Trans. Nucl. Sci. 62 (2015) 2283.

¹https://discovery.ucl.ac.uk/id/eprint/10158097/.

- [3] C.N. Burrous, A.J. Lieber and V.T. Zaviantseff, *Detection efficiency of a continuous channel electron multiplier for positive ions*, *Rev. Sci. Instrum.* **38** (1967) 1477.
- [4] M. Seah, Channel electron multipliers: quantitative intensity measurement efficiency, gain, linearity and bias effects, J. Electron Spectrosc. **50** (1990) 137.
- [5] G. Fraser, The ion detection efficiency of microchannel plates (MCPs), Int. J. Mass Spectrom. 215 (2002) 13.
- [6] M. Krems, J. Zirbel, M. Thomason and R.D. DuBois, Channel electron multiplier and channelplate efficiencies for detecting positive ions, Rev. Sci. Instrum. 76 (2005) 093305.
- [7] O. Sueoka, Detection efficiency of a continuous dynode electron multiplier (ceratron) for positrons, *Jpn. J. Appl. Phys.* **21** (1982) 702.
- [8] P.V. Schmidt et al., An efficient position sensitive detector for 3–30 kev positrons and electrons, Nucl. Instrum. Meth. A 376 (1996) 139.
- [9] S. Armitage, *Positronium ionisation in collision with He atoms*, Ph.D. Thesis, University College London, London U.K. (2002), https://discovery.ucl.ac.uk/id/eprint/10098018.
- [10] S. Armitage, D.E. Leslie, A.J. Garner and G. Laricchia, *Fragmentation of positronium in collision with He atoms*, *Phys. Rev. Lett.* **89** (2002) 173402.
- [11] M. Shipman et al., Absolute differential positronium-formation cross sections, Phys. Rev. Lett. 115 (2015) 033401.
- [12] S.E. Fayer et al., Differential positronium-formation cross sections for Ne, Ar, Kr, and Xe, Phys. Rev. A 100 (2019) 062709.
- [13] S.J. Brawley, J. Beale, S. Armitage, D.E. Leslie, Á. Kövér and G. Laricchia, *Fragmentation of positronium in collision with xenon*, *Nucl. Instrum. Meth. B* **266** (2008) 497.
- [14] M. Shipman, S. Brawley, D.E. Leslie, S. Armitage and G. Laricchia, *Production of collimated positronium by positron scattering from CO*₂, N₂ and Xe, Eur. Phys. J. D **66** (2012) 96.
- [15] D.A. Cooke, *Positron impact ionization of atoms and molecules*, Ph.D. Thesis, University College London, London U.K. (2010), https://discovery.ucl.ac.uk/id/eprint/624495.
- [16] D.A. Cooke, D.J. Murtagh and G. Laricchia, Simultaneous ionization and excitation of molecules by positron impact, Phys. Rev. Lett. **104** (2010) 073201.
- [17] G. Laricchia, Unpublished data, used in G. Laricchia et al., *Total positron-impact ionization and positronium formation from the noble gases*, *J. Phys. B* **35** (2002) 2525.
- [18] G. Laricchia et al., A statistical description of scattering at the quantum level, Sci. Rep. 8 (2018) 15056.
- [19] D.M. Newson, *Formation and scattering of positronium from atoms and molecules*, Ph.D. Thesis, University College London, London U.K., submitted (2022).
- [20] F. Bordoni, Channel electron multiplier efficiency for 10-1000 eV electrons, Nucl. Instrum. Meth. 97 (1971) 405.
- [21] Koninklijke Philips N.V., Electron Multipliers, Philips Components (1991).
- [22] A. Özen, A.J. Garner and G. Laricchia, *Rare gas solid moderator for Ps beam at ucl*, *Nucl. Instrum. Meth. B* **171** (2000) 172.
- [23] Dr. Sjuts Optotechnik GmbH, https://www.sjuts.com/index_english.html (2022).

- [24] F.A. Henkel, *Photoionisation detection of single* ⁸⁷*Rb-atoms using channel electron multipliers*, Ph.D. Thesis, University of Munich, Munich, Germany (2011), https://edoc.ub.uni-muenchen.de/13632/.
- [25] A.I. Williams et al., Moderation and diffusion of positrons in tungsten meshes and foils, J. Appl. Phys. 118 (2015) 105302
- [26] D.M. Newson, R. Kadokura, S.J. Brawley, M. Shipman and G. Laricchia, *Statistical nature of secondary electron emission*, in progress (2022).
- [27] J.R. Rumble eds., CRC Handbook of Chemistry and Physics, 102nd edition, CRC Press (2021).